Revisiting the F + HCl → HF + Cl reaction with a mutireference coupled-cluster method

Supplementary Material

Yuri Alexandre Aoto and Andreas Köhn

Institut für Theoretische Chemie, Universität Stuttgart, Pfaffenwaldring 55,

D-70569 Stuttgart, Germany

I. DETAILS ON THE FITTING PROCEDURE

The points used to fit the two-body terms are collected in the directory `two_body_points`, along with the weights used in the least square procedure. Data calculated at the following levels are given: icMRCCSD/aug-cc-pVTZ, icMRCCSD(T)/aug-cc-pV{T,Q,Z}Z and icMRCCSD(T)-cc/CBS.

The directory `three_body_points` contains the points used to fit the three-body terms. The three-body contribution corresponds to the total icMRCCSD(T)/aug-cc-pVTZ energy ($E(\mathbf{R})$), subtracted by the one and two body contributions:

$$V^{(3)}(\mathbf{R}) = E(\mathbf{R}) - V^{(1)} - V^{(2)}_{FH}(R_{FH}) - V^{(2)}_{HCl}(R_{HCl}) - V^{(2)}_{ClF}(R_{ClF})\,.$$

The file `three_body` contains the main set of points. The file `weights` have the weights used in the linear least squares fit. Points without an entry in this file received a default weight of 1.0. These weights were chosen after careful analysis of several cuts of the PES. We have discarded or given small weight for points where the PES showed a non-smooth behaviour. After removing the entries with weight 0.0, the number of points is 2983, as described in section IV of the main text. Higher weight was given for points close to the transition state, as follows. The distance d between the point and the transition state is calculated in perimetric coordinates. If $d < 0.25$, the point receives a weight of 10.0. If $0.25 \leq d < 0.5$, the point receives a weight of 7.5. If $0.5 \leq d < 0.75$, the point receives a weight of 5.0. If $0.75 \leq d < 1.0$, the point receives a weight of 2.0. However, the weights

given in the file `weights` have priority and this scheme is not applied for the collinear points, where the conical intersection seams are located.

All these points were chosen in the region close to the valley of the reaction F + HCl $\rightarrow$ HF + Cl, based on the known topology of the DHTSN PES. The selection was made in perimetric coordinates, using points roughly equally spaced on seven different λ-surfaces. See TCA 133, 1547 (2014) for a description of these surfaces in perimetric coordinates. Fig. S1 shows these points in perimetric coordinates. Compare it with the level surfaces depicted in Fig. 1 of the main text to see how these points cover the regions of the PES that are most important for the reaction.

The points in the other files received weights as follows. The file `three_body_close_TS` contains points around the transition state and these received a weight of 1.0. The file `three_body_extra` contains points at the H + FCl dissociation channel and in the far region of the other two dissociation channels. These points received a weight of 1.0. The file `three_body_low_lambda` contains points at a λ-surface in the repulsive wall of the H + FCl dissociation channel. These points received a weight of 1.0. The file `three_body_low_R` contains points for smaller internuclear distances and they received a weight of 0.001. The file `three_body_high_R` contains points in the atomic fragmentation region and they received a weight of 0.001. These last three sets of points were used to ensure that the fitted PES does not have unphysical oscillations in the corresponding regions. All these points are depicted in the Fig. S2-S4.

Subroutines to calculate the final PES are given in the directory `PES`.

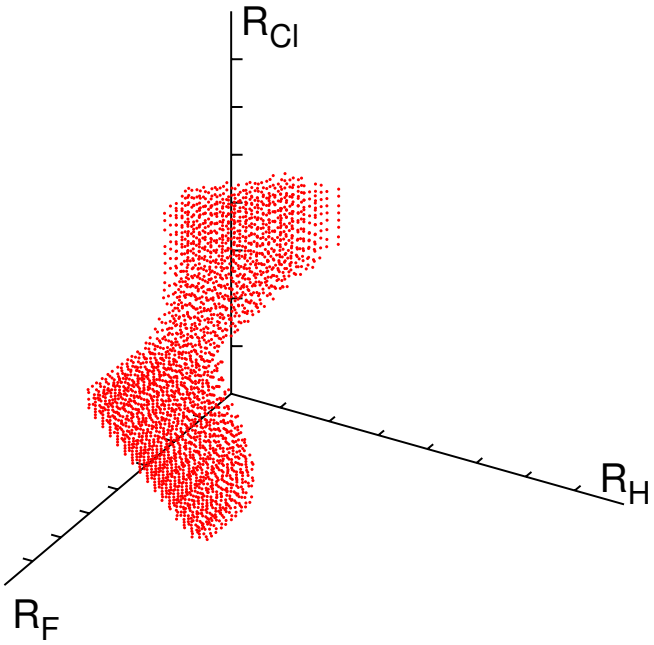

FIG. S1: Location of the points from file `three_body` in perimetric coordinates.

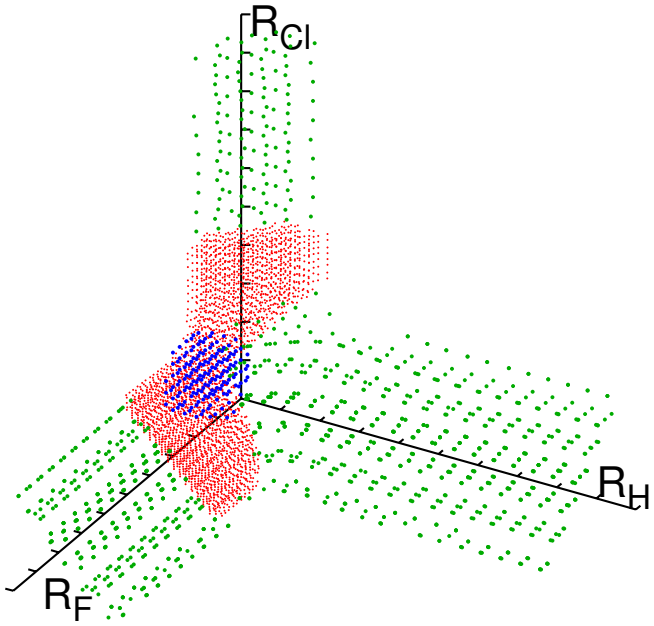

FIG. S2: Location of the points from files `three_body_close_TS` (blue dots) and `three_body_extra` (green dots) in perimetric coordinates. Points from file `three_body` are the small red dots.

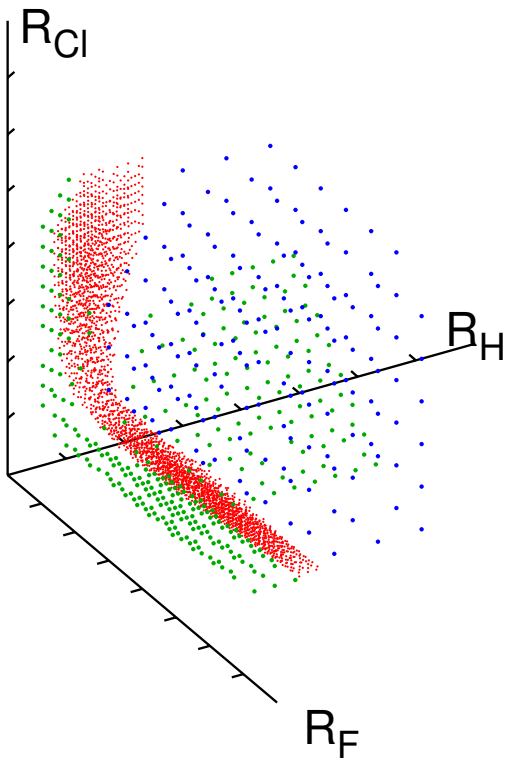

FIG. S3: Location of the points from files `three_body_low_R` (blue dots) and `three_body_high_R` (green dots) in perimetric coordinates. Points from file `three_body` are the small red dots.

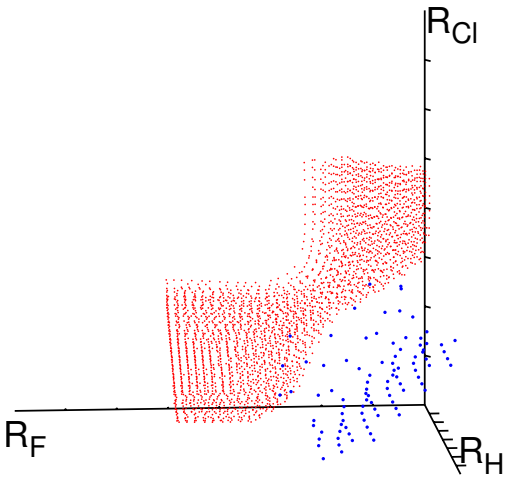

FIG. S4: Location of the points from file `three_body_low_lambda` (blue dots) in perimetric coordinates. Points from file `three_body` are the small red dots.

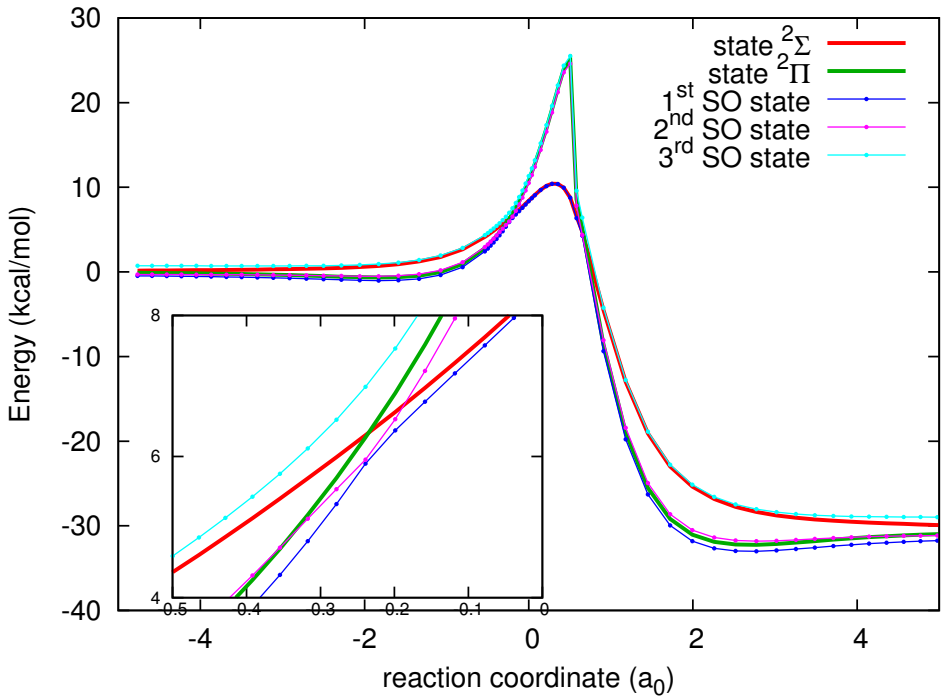

FIG. S5: Non-relativistic and spin-orbit coupled curves for the collinear minimum energy path, computed at the MRCI/aVTZ level. The inset shows the region close to the conical intersection at the entrance channel.

II. THE SPIN-ORBIT COUPLING AT THE MRCI LEVEL OF THEORY

To better understand the effect of spin-orbit coupling on the PES, we performed MRCI calculations with a triple zeta basis set. We investigated the three states that dissociate into the ground state F + HCl channel along the collinear minimum energy path (as in Fig. 4 of the main text). The spin-orbit coupling was calculated using the Breit-Pauli operator as implemented in Molpro. Figure S5 shows the results. At the MRCI/aVTZ level of theory this curve is quantitatively different from the icMRCCSD(T) counterpart, but all qualitative features are captured. In the figure, one can see the spin-orbit splitting in the entrance channel associated with the Fluorine atom. Only one of the two lowest energy states is reactive, giving rise to the multisurface statistical factor employed in the rate constant calculations, see Equation 14 of Tang *et al.* *JCP* **113**, 10105 (2000). On the other hand, the spin-orbit coupling practically does not affect the energy of the ground state close to the transition state. The lowering of the entrance channel energy effectively increases the barrier height by one third of the spin-orbit splitting of Fluorine.

Furthermore, the spin-orbit coupling lifts the degeneracy at the conical intersection. A close-up of the conical intersection in the entrance channel is shown in Figure S5. Effectively the spin-orbit coupling leads to a smooth transition between the $^2\Pi$ and the $^2\Sigma$ states, giving some support to our procedure of fitting a single reactive surface even for the collinear approach (as discussed in the main text).

III. TESTING THE PARAMETERS IN THE CHEMICAL DYNAMICAL CALCULATIONS

We performed test calculations to verify that the results on the dynamics are converged with respect to the calculation parameters. These are related to the size of the basis used to expand the wave function (the maximum internal energy, `emax`, the maximum rotational state, `jmax`, and the maximum helicity quantum number, `kmax`) and to the propagation of the coupled-channel equations (maximum hyperradius, `rmax`, and number of propagator sectors, `mtr`). For all calculations on the dynamics reported in the text, we used the same set of parameters of Li *et al.* [PCCP 2013, 15, 15347]. Fig. S6a shows the cumulative reaction probabilities (calculated with our new PES) for $J = 0$ and $J = 30$, calculated with this set of parameters. Probabilities calculated using variations of these parameters are shown in subfigures S6b-S6e and in Fig. S7, for the small range of energies shown by the rectangles in Fig. S6a (with the exception of Fig. S7b).

As one can see, results are well converged. This happens for the entire energy range for all parameters, except for `kmax`= 10 at higher energies, as shown in Fig. S7b. At `kmax`= 12 (the value used in the present work), however, results agree well with the ones for higher values of `kmax`. Since the value of `kmax` is restricted to be lower or equal than $min(J, j)$, no test is needed for $J = 0$.

Convergence of the vibrational distribution with respect to the total angular momentum is shown in Fig. S8. It shows the vibrational distribution for the single energy collision ($E_c = 4.3$ kcal mol^{-1} and ground rovibrational state, as in the hatched red bars in Fig. 5 of the main text) for several values of maximum total angular momentum (J_{max}). Results are well converged for $J_{max} = 99$, the truncation value used in this work.

(a) Cumulative reaction probability.

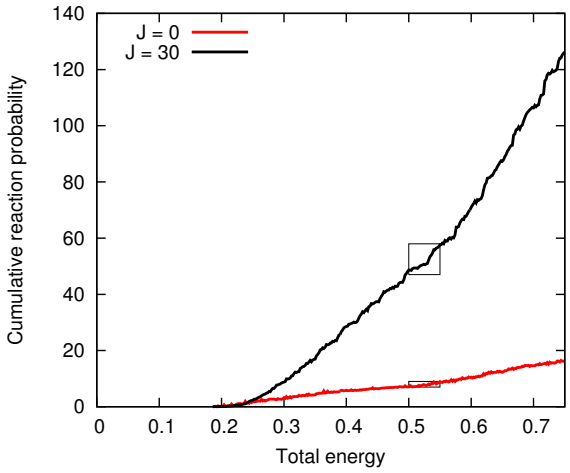

(b) Influence of `emax` for $J = 0$

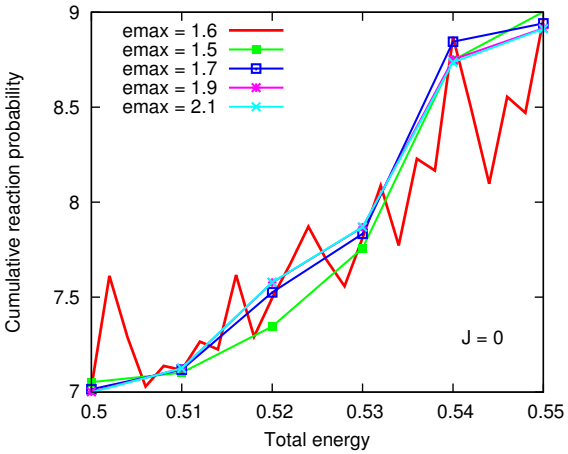

(c) Influence of `emax` for $J = 30$

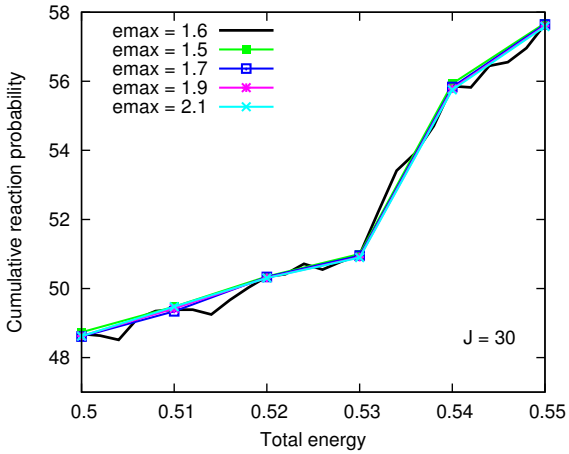

(d) Influence of `jmax` for $J = 0$

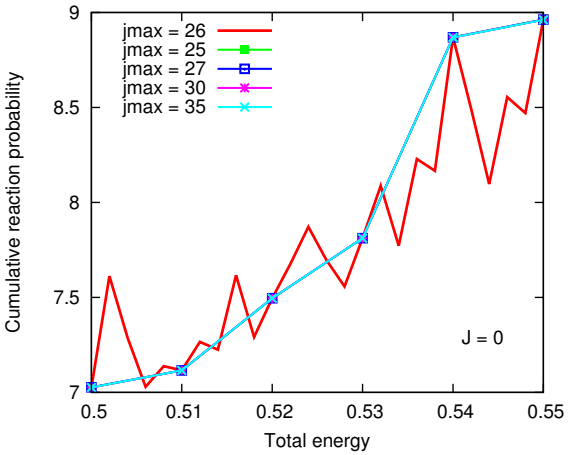

(e) Influence of `jmax` for $J = 30$

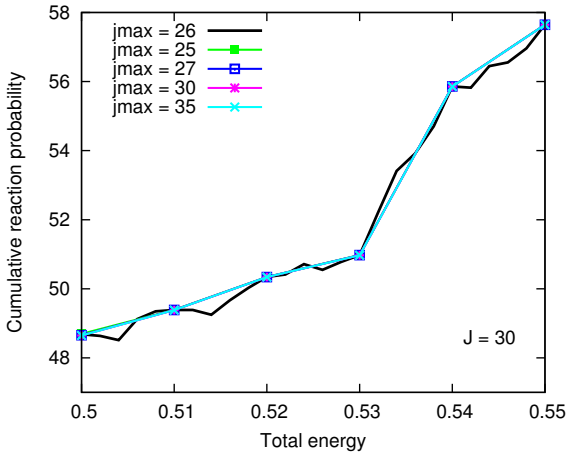

FIG. S6: Dependence of the results on the dynamics with the parameters the ABC code. The comparison is made for total angular momentum of $J = 0$ and $J = 30$.

(a) Influence of `kmax` for $J = 30$

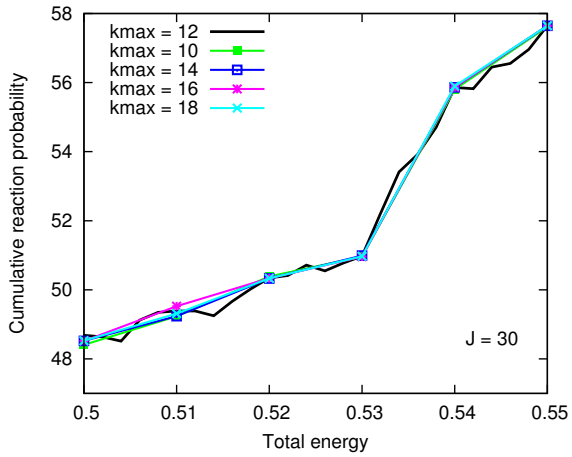

(b) Influence of `kmax` for $J = 30$

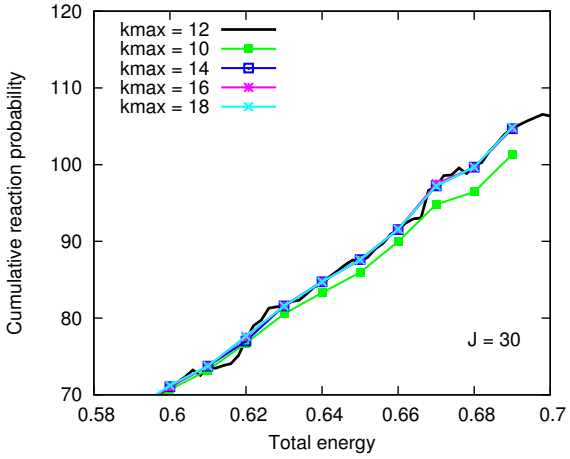

(c) Influence of `rmax` for $J = 0$

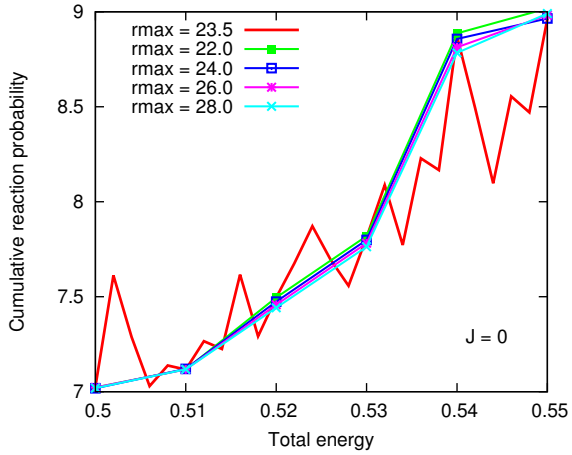

(d) Influence of `rmax` for $J = 30$

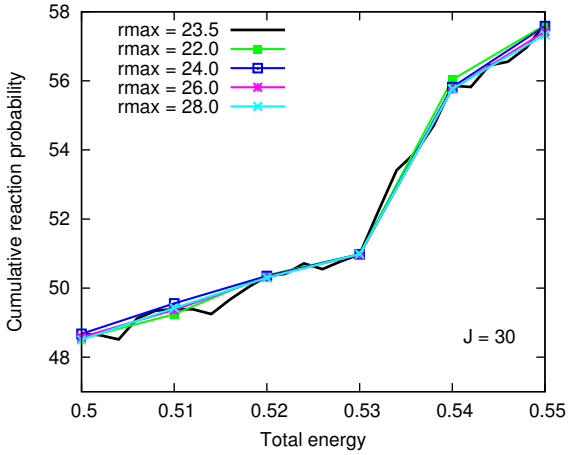

(e) Influence of `mtr` for $J = 0$

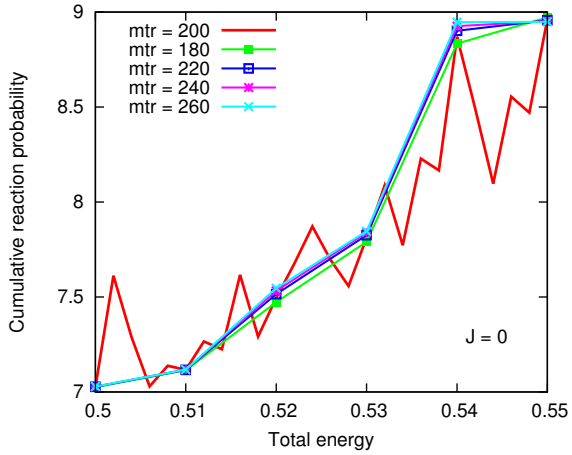

(f) Influence of `mtr` for $J = 30$

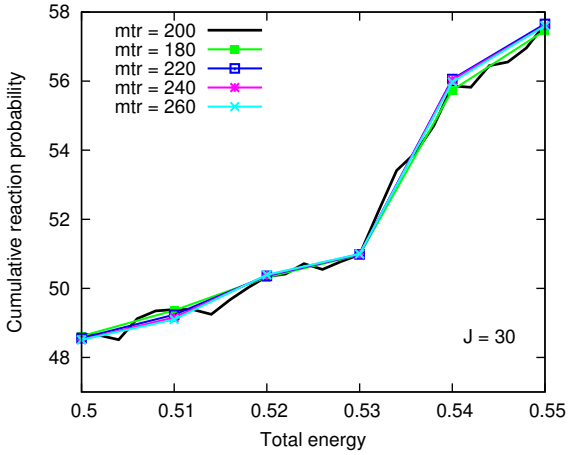

FIG. S7: Dependence of the results on the dynamics with the parameters the ABC code. The comparison is made for total angular momentum of $J = 0$ and $J = 30$.

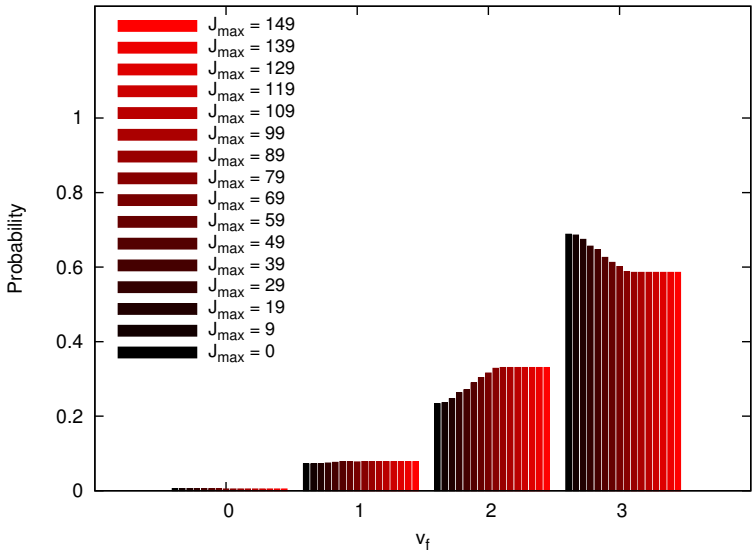

FIG. S8: HF vibrational distribution for collision energy of 4.3 kcal mol^{-1} and initial HCl rotational state $j_i = 0$.

IV. COLLISION ENERGY DISTRIBUTION

The collision energy distribution used in equation 8 of the article is simply given by the linear spline over the points in Table S1, obtained from the inset of Fig. 1 of JCP **127**, 114319 (2007).

TABLE S1: Collision energy distribution from the experiment of Zolot and Nesbit, JCP **127**, 114319 (2007)

E_c	$f_{ZN}(E_c)$	E_c	$f_{ZN}(E_c)$	E_c	$f_{ZN}(E_c)$	E_c	$f_{ZN}(E_c)$
1.041300	0.00000	2.670320	0.16853	3.984492	0.32391	5.805164	0.12669
1.328777	0.00120	2.766147	0.19602	4.162450	0.30837	6.065257	0.10578
1.698386	0.00837	2.903040	0.22829	4.408860	0.28626	6.393798	0.08486
1.862655	0.02809	3.012553	0.25638	4.668952	0.26175	6.694965	0.06155
2.109060	0.05319	3.176826	0.28566	4.860603	0.23785	7.146710	0.03944
2.259647	0.07888	3.368476	0.30418	5.038562	0.21395	7.625830	0.02390
2.423915	0.10817	3.491680	0.31912	5.284970	0.18646	8.118644	0.01255
2.533430	0.13626	3.669640	0.32928	5.490310	0.15777	8.693595	0.00000